

See discussions, stats, and author profiles for this publication at: <https://www.researchgate.net/publication/263951900>

# Sulfonated Poly(arylene sulfide sulfone nitrile) Multiblock Copolymers with Ordered Morphology for Proton Exchange Membranes

ARTICLE in MACROMOLECULES · SEPTEMBER 2013

Impact Factor: 5.8 · DOI: 10.1021/ma400889t

---

CITATIONS

11

READS

26

## 13 AUTHORS, INCLUDING:



Chang Hyun Lee

Seoul National University Hospital

157 PUBLICATIONS 2,768 CITATIONS

[SEE PROFILE](#)



James E McGrath

Virginia Polytechnic Institute and State Univer...

220 PUBLICATIONS 8,747 CITATIONS

[SEE PROFILE](#)



Robert B Moore

Virginia Polytechnic Institute and State Univer...

148 PUBLICATIONS 5,268 CITATIONS

[SEE PROFILE](#)



Louis A. Madsen

Virginia Polytechnic Institute and State Univer...

59 PUBLICATIONS 1,042 CITATIONS

[SEE PROFILE](#)

## Sulfonated Poly(arylene sulfide sulfone nitrile) Multiblock Copolymers with Ordered Morphology for Proton Exchange Membranes

Dong Won Shin,<sup>†,‡</sup> So Young Lee,<sup>†,‡</sup> Chang Hyun Lee,<sup>§,⊥</sup> Kwan-Soo Lee,<sup>§,#</sup> Chi Hoon Park,<sup>‡,%</sup> James E. McGrath,<sup>§</sup> Mingqiang Zhang,<sup>§</sup> Robert B. Moore,<sup>§</sup> Mark D. Lingwood,<sup>§</sup> Louis A. Madsen,<sup>§</sup> Young Taek Kim,<sup>||</sup> Inchul Hwang,<sup>||</sup> and Young Moo Lee\*,<sup>†,‡</sup>

<sup>†</sup>Department of Chemical Engineering, College of Engineering, Hanyang University, Seoul 133-791, Republic of Korea

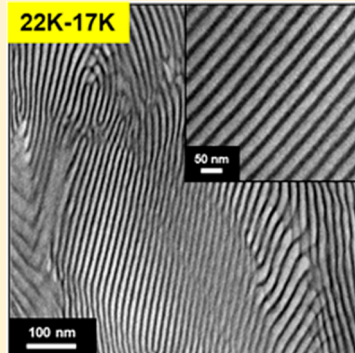
<sup>‡</sup>WCU Department of Energy Engineering, College of Engineering, Hanyang University, Seoul 133-791, Republic of Korea

<sup>§</sup>Macromolecules and Interfaces Institute and Department of Chemistry, Virginia Polytechnic Institute and State University, Blacksburg, Virginia 24061, United States

<sup>||</sup>Fuel Cell Team 3, Hyundai-Kia Motor Company, Yongin 446-716, Republic of Korea

### Supporting Information

**ABSTRACT:** Ordered morphologies in disulfonated poly(arylene sulfide sulfone nitrile) (SPSN) copolymers were generated via thermal annealing followed by multiblock copolymer synthesis. While SPSN random copolymers (R-SPSN) showed featureless morphologies, the SPSN multiblock copolymers (B-SPSN) exhibited cocontinuous lamellar morphologies with a center-to-center interdomain size of up to 40 nm. In spite of the well-ordered, interconnected hydrophilic domains, the water self-diffusion coefficient (e.g.,  $D = (0.7\text{--}2.0) \times 10^{-10} \text{ m}^2 \text{ s}^{-1}$ ) and proton conductivity (e.g.,  $\sigma = 0.16\text{--}0.20 \text{ S cm}^{-1}$ ) in deionized water at 30 °C through B-SPSN were lower than those of the corresponding R-SPSN (e.g.,  $D = (3.5\text{--}3.9) \times 10^{-10} \text{ m}^2 \text{ s}^{-1}$  and  $\sigma = 0.21 \text{ S cm}^{-1}$ ) due to the relatively lower water uptake of the B-SPSN after thermal annealing. The reduced water uptake of B-SPSN was beneficial to reduction of peroxide degradation rate. Thermal annealing produced significant gains in morphological ordering and finer control over desired membrane properties for proton conduction applications.



### INTRODUCTION

Proton exchange membrane fuel cells (PEMFCs) have been studied as an alternative power source for stationary and portable applications due to their high power density, excellent conversion efficiency, and environmental friendliness.<sup>1</sup> Proton exchange membranes (PEMs) are key components of PEMFCs. Perfluorosulfonic acid polymers (PFSAs) such as Nafion, Aciplex, and Flemion are widely used because of their excellent chemical and mechanical stabilities and high proton conductivity. However, there are several disadvantages of PFSAs such as high fuel permeabilities, difficult synthetic procedure, high cost, low glass transition temperature ( $T_g$ ), and environmental concerns of fluorine.<sup>2,3</sup>

Sulfonated aromatic polymers such as sulfonated poly(arylene ether)s (SPAEs)<sup>4–7</sup> and sulfonated polyimides (SPIs)<sup>8–11</sup> have been extensively investigated due to their excellent thermal stabilities and low fuel permeabilities to overcome the drawbacks of PFSAs. However, these polymers have relatively low proton conductivity than PFSAs because rigid hydrocarbon polymer chains hinder hydrophilic ionic channel formation.<sup>12</sup> For these reasons, many researches of block copolymers,<sup>13–20</sup> pendant or comb-shaped copoly-

mers,<sup>1,10,21–23</sup> and highly sulfonated copolymers<sup>24–26</sup> have been studied to improve proton conductivity.

Among them, sulfonated block copolymers with well-defined morphologies have recently received much attention.<sup>27</sup> Similar to other block copolymers, sulfonated block copolymers exhibit independent combinations of intrinsic properties that originate from their block components, which have controlled molecular weights and different chemical architectures. Thus, careful design of block components at the molecular level can be a successful method to achieve copolymer characteristics suitable for target applications. Furthermore, the physical and chemical properties of sulfonated block copolymers, including their morphologies, are largely influenced by the copolymer processing conditions adopted after synthesis.<sup>18</sup>

Sulfonated polymers are vulnerable to polymer degradation when exposed to the harsh operation conditions needed for energy generation.<sup>28</sup> In this regard, thermal annealing may be a good solution to further improve the stabilities of amorphous sulfonated block copolymers. The synthesis of sulfonated block

**Received:** April 29, 2013

**Revised:** September 9, 2013

**Published:** September 17, 2013

copolymers with semicrystalline structure, which leads to excellent stability of polymer membrane, is difficult, especially those composed of wholly aromatic backbones, since bulky  $-SO_3H$  groups prevent the copolymer chains from being packed in an ordered fashion. Moreover, the presence of semicrystalline domains results in insolubility in most organic solvents at the temperatures required for polymer synthesis and processing.<sup>29</sup> For these reasons, thermal annealing to reduce water uptake and produce well-ordered morphology is an effective method to enhance mechanical properties of sulfonated polymer membranes.<sup>30,31</sup>

In the present study, we demonstrate the formation of well-ordered morphology via the thermal treatment of amorphous disulfonated poly(arylene sulfide sulfone nitrile) multiblock copolymers (B-SPSN) depressed near their glass transition temperatures.<sup>31</sup> The sulfide group ( $-S-$ ) has a rotational conformational energy lower than the ether ( $-O-$ ) linkage.<sup>32</sup> Pendant nitrile ( $-CN$ ) groups can form strong dipolar interactions with  $-SO_3H$  and/or  $-CN$  groups in SPSN chains.<sup>33–36</sup> Thus, B-SPSNs possess unique properties such as good resistance to thermal and chemical stimuli, excellent mechanical toughness, and easy processability for organic–inorganic composite formation.<sup>5,25,37–39</sup> Here, we report the influence of the morphological transition of B-SPSN on water and proton transport behavior after thermal treatment.

## EXPERIMENTAL DETAILS

**Materials.** 4,4'-Thiobisbenzenethiol (TBBT) and 2,6-dichlorobenzonitrile (DCBN) were purchased from Sigma-Aldrich and purified by recrystallization. 4,4'-Dichlorodiphenyl sulfone (DCDPS), decafluorobiphenyl (DFBP), and potassium carbonate were provided by Alfa Aesar (Ward Hill, MA) and used as received. 1-Methyl-2-pyrrolidinone (NMP), toluene, and all other solvents and reagents were reagent grade and were used without further purification. 3,3'-Disulfonated-4,4'-dichlorodiphenyl sulfone (SDCDPS) was synthesized and purified according to a procedure reported elsewhere.<sup>40</sup>

**Synthesis of Thiol-Terminated Sulfonated Poly(arylene sulfide sulfone) (SPAS) Hydrophilic Oligomer.** Fully disulfonated poly(arylene sulfide sulfone) (SPAS) hydrophilic oligomers with different molecular weights were synthesized by a nucleophilic aromatic substitution reaction. To a 250 mL four-necked round-bottom flask equipped with a nitrogen inlet, thermometer, mechanical stirrer, Dean–Stark trap, and condenser, 2.50 g (10.0 mmol) of TBBT, 4.77 g (9.7 mmol) of SDCCDPS, and 1.66 g (12.0 mmol) of potassium carbonate were introduced as a monomer and catalyst. NMP (70 mL) and toluene (30 mL) were added as a solvent and an azeotrope reagent. The reaction mixture was stirred under a nitrogen atmosphere at room temperature for 30 min and refluxed at 140 °C to remove water, which causes chain termination. After removing all water and azeotrope reagent, the reaction temperature was elevated to 170 °C, and the reaction was continued for 24 h to obtain the target molecular weight. The oligomer solution was cooled to room temperature, filtered to remove the salt, and then precipitated into 2-propanol. The precipitated oligomer was filtered and washed with 2-propanol several times to remove remaining solvent and then dried under vacuum at 100 °C.

**Synthesis of Thiol-Terminated Poly(arylene sulfide nitrile) (PASN) Hydrophobic Oligomer.** A series of unsulfonated poly(arylene sulfide nitrile) (PASN) oligomers with various molecular weights were synthesized. 3.76 g (15.0 mmol) of TBBT, 2.54 g (14.8 mmol) of DCBN, and 2.59 g (18.0 mmol) of potassium carbonate were charged in a four-necked round-bottom flask, equipped with a nitrogen purge, thermometer, mechanical stirrer, Dean–Stark trap, and condenser. NMP (60 mL) and toluene (20 mL) were added to the flask. The reaction mixture was stirred under a nitrogen atmosphere at room temperature for 30 min and heated to 140 °C to remove water. After removing all water and toluene, the reaction

was allowed to proceed at 170 °C for 24 h to obtain the target molecular weight. The same precipitation and purification process as used for the SPAS oligomer was applied for PASN oligomers.

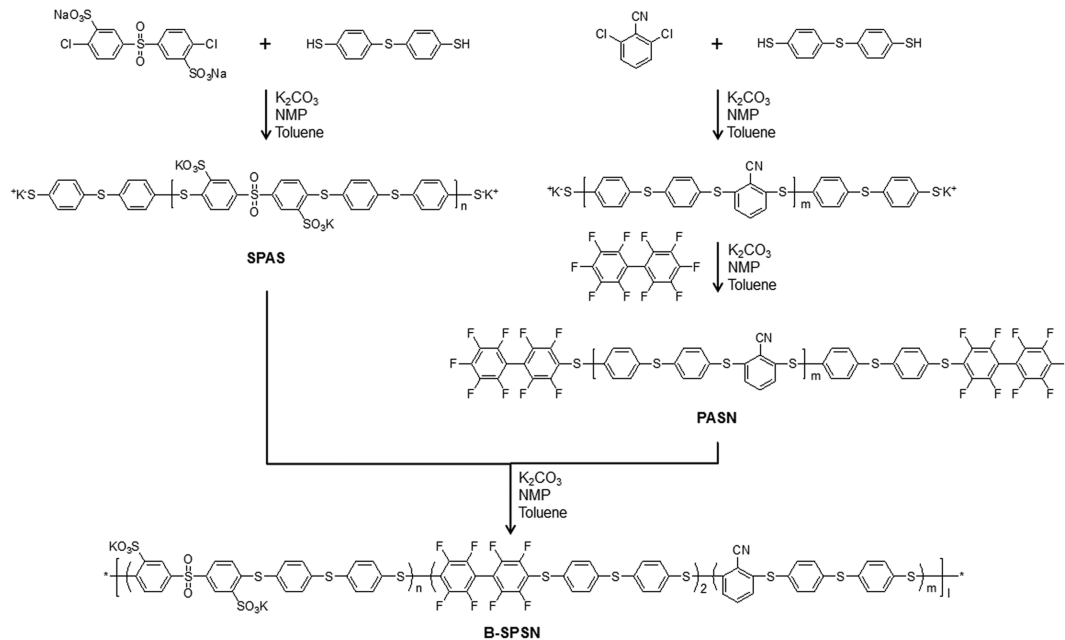
**End-Capping of Thiol-Terminated PASN Hydrophobic Oligomer with DFBP.** Thiol-terminated PASN hydrophobic oligomers were end-capped with DFBP to produce a reactive site for coupling with thiol-terminated SPAS hydrophilic oligomers. A typical end-capping procedure is as follows. 1.0 mmol of PASN oligomer and 0.28 g (2.0 mmol) of potassium carbonate were charged to a 500 mL four-neck round-bottom flask, equipped with a nitrogen purge, thermometer, mechanical stirrer, Dean–Stark trap, and condenser. NMP (200 mL) was added to the flask, and all components were dissolved at room temperature for 30 min before toluene (70 mL) was introduced. The reaction mixture was allowed to reflux at 140 °C to azeotropically remove the water. After removing all water and toluene from the system, the reaction temperature was decreased to 100 °C, and 2.00 g (6.0 mmol) of DFBP was then added and the reaction allowed to proceed for 12 h. The solution was cooled to room temperature and filtered. The filtered solution was precipitated into methanol. The DFBP end-capped PASN oligomer was dried at 100 °C under vacuum for 24 h.

**Synthesis of Hydrophilic–Hydrophobic Block Copolymers.** Hydrophilic–hydrophobic block copolymers with different chain lengths were synthesized via a coupling reaction between thiol-terminated hydrophilic oligomer (SPAS) and DFBP end-capped hydrophobic oligomer (PASN). A typical coupling reaction was performed as follows. 1.0 mmol of SPAS oligomer, 0.28 g (2.0 mmol) of potassium carbonate, and NMP (200 mL) were charged to a 500 mL four-neck round-bottom flask equipped with a nitrogen purge, thermometer, mechanical stirrer, Dean–Stark trap, and condenser. The mixture was dissolved at room temperature before toluene (70 mL) was added. The reaction mixture was heated to 140 °C with refluxing toluene. After removing toluene, the reaction temperature was dropped to 100 °C and 1 mmol of DFBP end-capped PASN oligomer was added. The coupling reaction proceeded for 24 h to obtain block copolymer. The final polymer solution was cooled to room temperature and filtered. The filtered polymer solution was coagulated in a mixture of 2-propanol and water. The precipitated block copolymer was filtered and washed with water several times to remove remaining solvent and then dried under vacuum at 100 °C for 24 h.

**Membrane Preparation and Acidification.** The dried SPSN copolymers were dissolved as 15 wt % solution in DMAc at room temperature. The polymer solution was filtered using a 0.45  $\mu$ m PTFE filter and cast onto glass plates, with final membrane thickness in the range 50–65  $\mu$ m. After solution casting, R-SPSN and B-SPSN solutions were dried under two different thermal protocols: one set was dried at 120 °C under vacuum for 2 days, while the other set was dried at 220 °C under vacuum for an additional 2 days immediately after pristine sample formation. Each set was immersed in deionized water for 1 week after the thermal treatments. The deionized water was exchanged on a daily basis. Each salt-form membrane was then acidified using boiling 0.5 M H<sub>2</sub>SO<sub>4</sub> for 2 h, followed by boiling in deionized water for another 2 h to obtain proton-form ( $-SO_3^-H^+$ ) membrane. Nafion 212 was purchased from DuPont and used as received.

**Characterization and Measurements.** Proton nuclear magnetic resonance spectroscopic (<sup>1</sup>H NMR) analysis was conducted on a 300 MHz Bruker AV 300 spectrometer using DMSO-*d*<sub>6</sub> as a solvent to confirm the chemical structures of the oligomers and block copolymers.

Gel permeation chromatography (GPC) was performed using a Waters 2414 refractive index detector equipped with Styragel HR 3 and 4 columns to verify the molecular weight of the oligomers and block copolymers. NMP containing 0.05 M LiBr was used as the mobile phase, and the column temperature was maintained at 50 °C in order to reduce the viscosity of NMP. LiBr was used to control ionic aggregates associated with the sulfonated copolymers and minimize the ionic effect.<sup>7</sup>

**Scheme 1.** Synthetic Route of Sulfonated Poly(arylene sulfide sulfone nitrile) (B-SPSN) Block Copolymer

In-situ small-angle X-ray scattering (SAXS) was performed at Advanced Photon Source (APS), Argonne National Laboratory (Beamline 5-ID DND-CAT). The wavelength of X-ray is 0.072 93 nm. Scattering from a silver behenate standard was used to calibrate the sample-to-detector distance, and the sample-to-detector distance was 2974 mm. SAXS images were obtained using a low-noise, Mar USA Inc., 162 mm, MarCCD camera, with a 4 s exposure time. All SAXS data had been corrected for sample thickness, sample transmission, and background scattering. All SAXS data were analyzed using the in-house software package provided in APS to obtain radically integrated SAXS intensity versus scattering vector  $q$  (SAXS), where  $q = (4\pi/\lambda) \sin(\theta)$ ,  $\theta$  is one-half of the scattering angle, and  $\lambda$  is the wavelength of X-ray.

For the TEM observation, the membranes were stained with lead ions ( $Pb^{2+}$ ) by immersion in a 0.5 M lead acetate aqueous solution, rinsed with deionized water, and dried in a vacuum oven. The stained membranes were embedded in epoxy resin, microtomed to a thickness of 70 nm using a RMCMTX Ultra microtome, and placed on copper grids. The TEM images were taken using a Carl Zeiss LIBRA 120 energy filtering transmission electron microscope at an accelerating voltage of 120 kV.

Pulsed-field-gradient (PFG) NMR was conducted at 25 °C on a 400 MHz Bruker Avance III spectrometer equipped with a Bruker MicroS triple-axis-gradient microimaging probe and a 10 mm  $^1H$  radio-frequency coil. The membranes were cut into 5 mm × 5 mm square pieces, stacked together to create a total mass between 7 and 25 mg, secured with Teflon tape, and soaked in deionized water for at least 24 h. Before measurement, the membranes were removed from the water, blotted to remove excess water on the surface, wrapped in LDPE food-sealing wrap, and transferred to a custom-built sample cell with a low dead volume and excellent sealing characteristics.<sup>16</sup> The pulsed-gradient stimulated echo sequence (PGSTE) was used for diffusion measurements both in the in-plane and through-plane directions with a gradient pulse duration of  $\delta = 2$  ms, diffusion time  $\Delta = 50$  ms, and 16 gradient steps. Maximum gradient strengths between 120 and 230 G cm<sup>-1</sup> were used, and the data were fit to the well-known Stejskal–Tanner equation to yield the self-diffusion coefficient of the water absorbed in the material.<sup>41</sup> The polymeric  $^1H$  nuclei have unfavorable relaxation properties (short  $T_2$ ) and are not observed in PFG diffusion measurements. The error in measured diffusion coefficient is estimated at  $\pm 4\%$  of the measured value.

Recently, Kim and Pivovar emphasized the use of volume-based parameters because proton conduction occurs over large length scales and polymer membranes have significantly different densities that are likely better represented by volume-based parameters than mass-based parameters.<sup>42</sup> The membrane density of dry and wet samples were measured by the floatation method using a microbalance and with 2,2,4-trimethylpentane as a reference liquid. The IEC based on weight (IEC<sub>w</sub>) was measured using a conventional titration method. The volume-based IEC of wet membrane (IEC<sub>v(wet)</sub>) were obtained by multiplying the wet membrane density by the IEC<sub>w</sub> values. The hydrated molar volume per charge of fully hydrated membrane (MVC<sub>(wet)</sub>) was calculated from van der Waals volume increments of the composing atoms or structural groups of sulfonated polymers and membrane water uptake. The percent conducting volume (PCV), which is the ratio of the volume of water uptake to the acid volume concentration, was obtained from the MVC and the hydration number. The mass-based water uptake (WU<sub>w</sub>) was calculated from the mass difference between the dry and wet states. The volume-based water uptake (WU<sub>v</sub>) was calculated from the dimensional change between the dry and hydrated states. The dimensions of the membranes were measured using a microscope, and a thickness gauge was used for thickness measurement.

The chemical stability of B-SPSN, R-SPSN, and Nafion was measured using Fenton's reagent (3 wt % H<sub>2</sub>O<sub>2</sub> aqueous solution containing 2 ppm Fe<sup>2+</sup>). The retained weight (RW) was calculated from the membrane weight before and after immersion in Fenton's reagent at 80 °C for 1 h (RW<sub>1h</sub>) and 3 h (RW<sub>3h</sub>). The dissolution time ( $\tau$ ) was measured by observing the immersed membrane until it dissolved completely at 80 °C.

The proton conductivity of the membranes was measured at 80 °C using homemade cell connected to a PEMFC single cell test station (CNL, Seoul, Korea) as a function of relative humidity. The humidity was controlled by changing the temperature of the humidifier and the single cell. The membrane samples were equilibrated at each relative humidity condition (30 and 90% RH) for 6 h. The proton conductivity was calculated from the resistance between the working and the counter electrode. The resistance of the membranes was measured over a frequency range from 100 mHz to 100 kHz using an electrode system connected with an impedance/gain-phase analyzer (Solartron 1260, Farnborough, Hampshire, UK) and an electrochemical interface (Solartron 1287).

The membrane electrode assembly was prepared by hot-pressing the membrane with the catalyst-loaded gas diffusion layer. The catalyst ink was composed of 20 wt % Pt/C (Johnson Matthey, UK) and 20 wt % Nafion ionomer (Sigma-Aldrich, St. Louis, MO). The catalyst was loaded on the gas diffusion layer by the screen printing method. The PEMFC single cell test was performed at 80 °C under 100% and 30% relative humidity and atmospheric conditions using a fuel cell test station (WonATech, Seoul, Korea). The active area of the MEAs was 5 cm<sup>2</sup> with a 0.3 mg cm<sup>-2</sup> Pt loading, and 100 sccm of hydrogen and 300 sccm of air were used as a fuel and oxidant. Before single cell performance measurement, a cyclic test was implemented at 80 °C under 100% relative humidity by changing the voltage (OCV–0.6 V–0.4 V, each step was maintained for 1 min) for 5 h to activate MEAs.

## RESULTS AND DISCUSSION

**Synthesis and Characterization of Hydrophilic and Hydrophobic Oligomers and Block Copolymers.** Fully sulfonated poly(arylene sulfide sulfone) (SPAS) hydrophilic oligomers with different molecular weights were synthesized by polycondensation using various feed ratios of 3,3'-disulfonated-4,4'-dichlorodiphenyl sulfone (SDCDPS) and 4,4'-thiobisbenzenethiol (TBBT), as shown in Scheme 1. An excess of TBBT was used to control the molecular weight and terminate oligomer chain end functionality. A dark purple powder which was soluble in water was obtained.

The preparation of non-sulfonated hydrophobic oligomers was performed in a two-step process comprised of an initial polycondensation reaction of TBBT with 2,6-dichlorobenzonitrile (DCBN) yielding poly(arylene sulfide nitrile) (PASN) and end-capping using DFBP to terminate the hydrophobic oligomers with a halide. The first step was performed with an excess of TBBT, just as in the SPAS synthesis procedure, while the second step was performed with an excess of DFBP to prevent chain extension. DFBP has been suggested to be useful to accelerate the reaction when coupled with hydrophilic oligomers.

Block copolymers were successfully synthesized by a coupling reaction between thiol-terminated hydrophilic oligomers and fluorine-terminated hydrophobic oligomers at a low temperature. Each oligomer was added in an equimolar ratio, and the yield was typically in the range of 90%. Sulfonated block copolymers were soluble in polar aprotic solvents such as NMP, DMSO, and DMAc.

The chemical structures of both oligomers and block copolymers were confirmed by <sup>1</sup>H NMR spectroscopy in DMSO-*d*<sub>6</sub>, as shown in Figure 1. Protons located at the ortho-position of the sulfonic acid group were assigned to the peak at 8.3 ppm, which indicated the successful synthesis of SDCDPS. While protons on the TBBT moieties located at the end of the hydrophilic oligomers were assigned to the peak at 6.8 ppm, those of hydrophobic oligomers were not clearly seen due to the DFBP end-capping. After coupling the hydrophilic oligomer with the hydrophobic oligomer, sulfonic acid groups and linkage groups were still present, resulting in complete synthesis of block copolymers without any chain cleavage or decomposition.

The number-average molecular weight of hydrophilic and hydrophobic oligomers was determined by GPC in NMP containing 0.05 M LiBr. Both hydrophilic and hydrophobic oligomers were successfully synthesized with target molecular weights from 17 to 27 kg mol<sup>-1</sup>. The structure of the block copolymers changed with the chain length of the oligomers.

**Solvent-Assisted Thermal Annealing Effect on Morphology.** The nanophase morphologies of Nafion, R-SPSN,

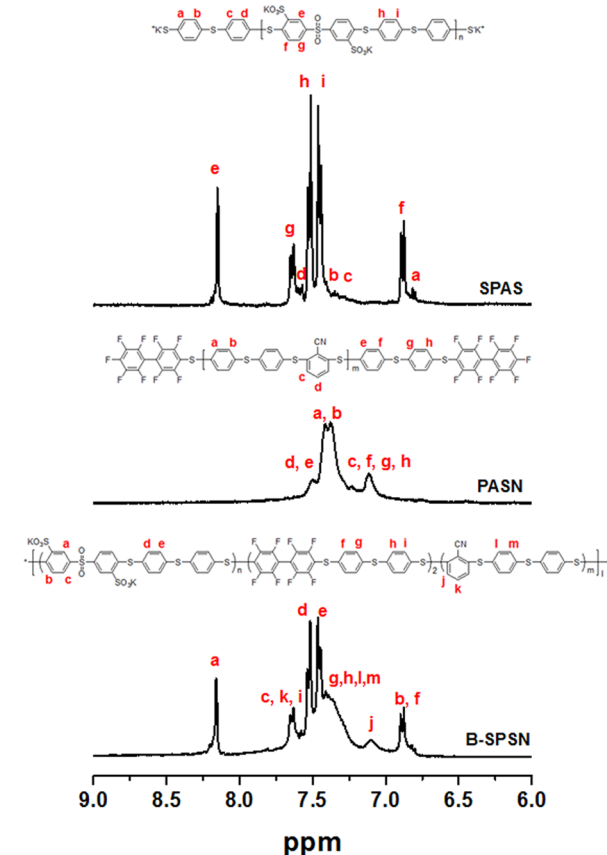


**Figure 1.** <sup>1</sup>H NMR spectra of hydrophilic (SPAS) and hydrophobic (PASN) oligomers and sulfonated poly(arylene sulfide sulfone nitrile) (B-SPSN) block copolymer.

and B-SPSN were analyzed by transmission electron microscopy (TEM), as shown in Figure 2. Nafion is composed of a short main chain and a long side chain that can be easily

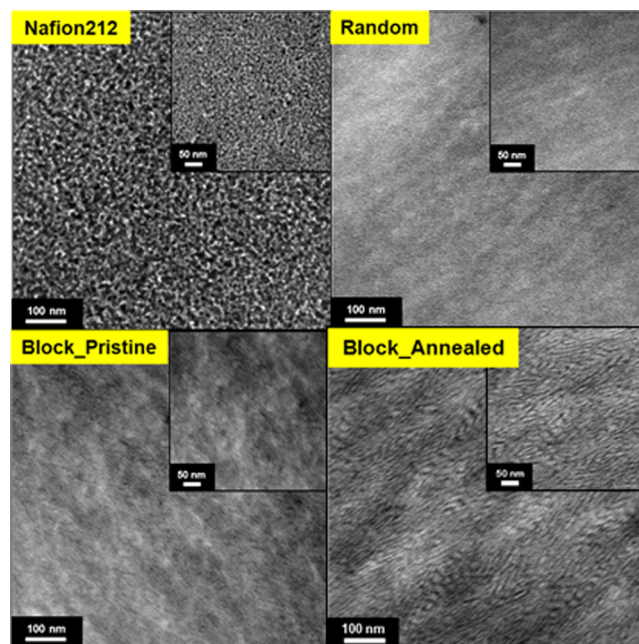


**Figure 2.** TEM images of Nafion, R-SPSN, and B-SPSN before and after thermal annealing.

aggregated, resulting in well-defined hydrophilic (dark region) and hydrophobic (bright region) phase separation. However, R-SPSN showed a homogeneous phase image due to the randomly distributed hydrophilic and hydrophobic domains in the polymer chain. The phase separation behavior of B-SPSN changed significantly after thermal annealing. Although pristine B-SPSN exhibited a weakly phase-separated image, the thermally annealed B-SPSN showed a well-connected morphology.

**Morphology Effect on Transport Behavior.** The small-angle X-ray scattering (SAXS) profiles of the thermally annealed B-SPSN and R-SPSN are presented in Figure 3.

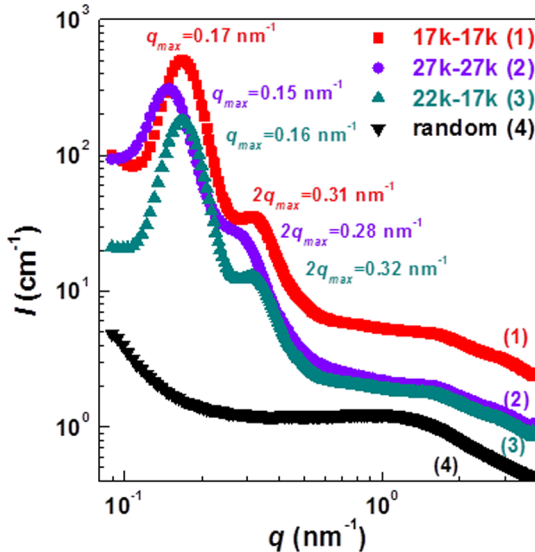


Figure 3. Synchrotron SAXS patterns of the B-SPSN and R-SPSN.

The B-SPSN composed of equal or unequal hydrophilic and hydrophobic block lengths exhibited noticeable scattering maxima, while the R-SPSN showed a featureless profile. All B-SPSN exhibited two different scattering peaks: a Gaussian peak (represented as  $q_{\max}$ ) and a weak second-order peak (represented as  $2q_{\max}$ ). The  $2q_{\max}$  value was almost 2 times higher than the  $q_{\max}$  value (e.g.,  $q_{\max} = 0.17 \text{ nm}^{-1}$  and  $2q_{\max} = 0.31 \text{ nm}^{-1}$  for the 17K-17K sample), which can be attributed to the well-ordered lamellar structure.<sup>43</sup> The SAXS scattering profiles of the B-SPSN confirmed the presence of a lamellar microstructure with a long-range periodicity.

As the length of the hydrophilic or hydrophobic block increased, the Gaussian peak shifted to lower  $q$  values, indicating an increase in the interdomain distance. Comparing the 17K-17K and 22K-17K samples, the  $q_{\max}$  value decreased from 0.17 to 0.16  $\text{nm}^{-1}$ , indicating that the interdomain distance increased from 37 to 39 nm with increasing hydrophilic chain length. In addition, the  $q_{\max}$  value decreased from 0.16 to 0.15  $\text{nm}^{-1}$  ( $d_{\text{Bragg}} = 39$  to 42 nm) as the hydrophilic and hydrophobic chain length increased from 22K-17K to 27K-27K. This could be due to the thicker hydrophobic domain causing an expansion of the Bragg distance of the hydrophilic region. The corresponding TEM images shown in Figure 4 further support the B-SPSN and R-SPSN SAXS results. A distinct hydrophilic–hydrophobic phase-separated morphology was observed in the B-SPSN with increased block length. The 22K-17K sample, represented as a black line, exhibited a very clear and large hydrophilic domain

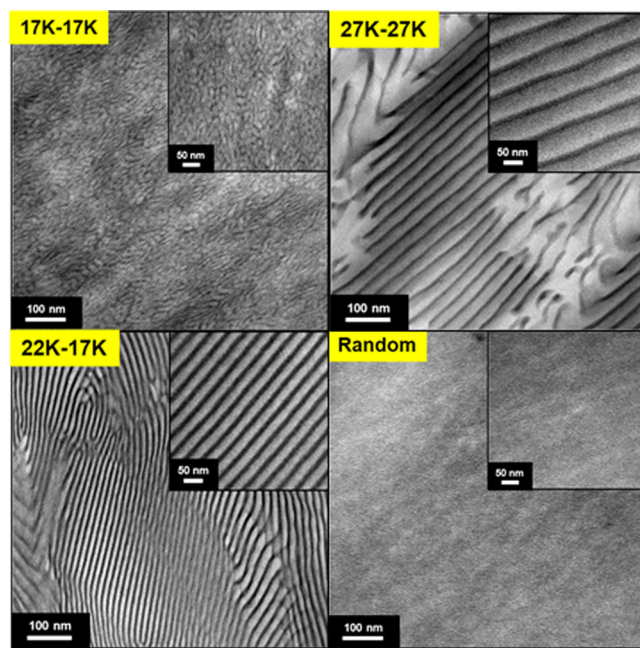


Figure 4. TEM images of the B-SPSN and R-SPSN.

by lead staining as compared to the 17K-17K sample. The 27K-27K sample showed a thicker white hydrophobic domain compared to the 22K-17K sample. The featureless SAXS profile of the R-SPSN supports a homogeneously distributed morphology.

The water self-diffusion coefficient ( $D$ ) was measured using pulsed-field-gradient (PFG) NMR to evaluate effects of the induced morphology on transport properties. PFG NMR was performed using a simple pulsed-gradient stimulated echo (PGSTE) sequence and a home-built sample cell as described previously.<sup>16</sup> The water self-diffusion coefficients  $D_{\perp}$  (through-plane) and  $D_{\parallel}$  (in-plane) are shown in Figure 5. R-SPSN

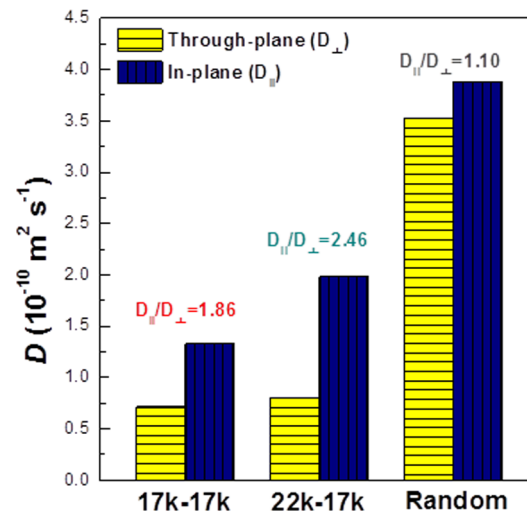


Figure 5. In-plane and through-plane water self-diffusion coefficients of saturated B-SPSN and R-SPSN measured by PFG NMR. Block copolymer membranes are clearly anisotropic due to the lamellar morphology aligned in the membrane plane. Errors in  $D$  are  $\pm 4\%$ , with a slightly larger error (+4%/-10%) for the random copolymer membrane, due to a minor restricted diffusion effect (see Supporting Information). Thus, the R-SPSN is isotropic to within errors.

**Table 1.** Density and Proton Conducting Parameters of Nafion, Thermally Annealed B-SPSN, and R-SPSN for PEM

sample	density <sub>(dry)</sub> [g cm <sup>-3</sup> ]	density <sub>(wet)</sub> [g cm <sup>-3</sup> ]	IEC <sub>w</sub> [mequiv g <sup>-1</sup> ]	IEC <sub>v(wet)</sub> [mequiv cm <sup>-3</sup> ]	WU <sub>w</sub> [wt %]	WU <sub>v</sub> [vol %]	MVC <sub>(wet)</sub> [cm <sup>3</sup> mol <sup>-1</sup> ]	PCV
17K-17K	1.56	1.52	1.58	2.40	39	43	702	0.36
27K-27K	1.52	1.47	1.58	2.32	40	45	694	0.36
22K-17K	1.63	1.59	1.71	2.72	56	59	723	0.45
random	1.49	1.44	1.52	2.19	88	95	1037	0.56
Nafion	1.98	1.72	0.90	1.55	45	85	742	0.36

exhibited much higher diffusion coefficients than B-SPSN. This is likely due to the lower water uptake of B-SPSN (88 wt % water for random vs 39 wt % for 17K-17K and 56 wt % for 22K-17K blocks), which hinders water and proton transport through the hydrophilic or liquid-like domain.<sup>44,45</sup> The water self-diffusion coefficient depends strongly on water uptake in ionomer membranes.<sup>16,46</sup> In particular, the  $D_{\parallel}$  of the block copolymers increased with hydrophilic chain length due to the formation of increasingly well-ordered hydrophilic channels. Moreover, R-SPSN showed nearly isotropic transport behavior to within errors ( $D_{\parallel}/D_{\perp} = 1.10$ ; see also Supporting Information discussion on minor restricted diffusion due to membrane interfaces), whereas B-SPSN showed strongly anisotropic transport behavior, with a  $D_{\parallel}/D_{\perp}$  up to 2.46.  $D_{\parallel}$  was always higher than  $D_{\perp}$ , suggesting that the nanophase-separated lamellar morphology was arranged in the plane of the membrane. This in-plane aligned lamellar morphology of the annealed B-SPSN arose from the membrane casting procedure and was likely also affected by surface interactions.

**Proton Conducting Parameters and Chemical Stabilities.** The well-ordered lamellar morphology of B-SPSN gives it great potential for use in proton exchange membranes (PEMs) in fuel cell applications. The nanoscale and well-connected hydrophilic ion conducting channel morphology is a key factor affecting PEM performance. The PEM properties of Nafion, thermally annealed B-SPSN, and R-SPSN were measured to estimate their fuel cell performance, and the results are shown in Table 1. While the IEC<sub>w</sub> values of B-SPSN and R-SPSN were similar, the IEC<sub>v(wet)</sub> values of B-SPSN were much larger than those of R-SPSN and Nafion due to their low water uptake and swelling ratios. Additionally, the B-SPSN showed lower MVC<sub>(wet)</sub> and PCV values than the R-SPSN.

The chemical stability of Nafion, thermally annealed B-SPSN, and R-SPSN membranes are also shown in Table 2. The

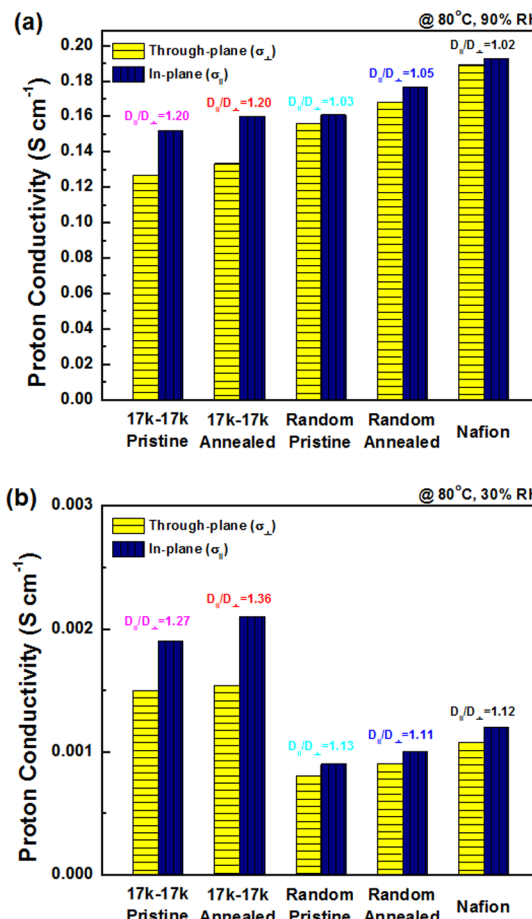
**Table 2.** Oxidative Stability of Nafion, Thermally Annealed B-SPSN, and R-SPSN

sample	RW <sub>1h</sub> [%]	RW <sub>3h</sub> [%]	$\tau$ [h]
17K-17K	103	95	14
27K-27K	104	95	15
22K-17K	104	93	12
random	107	89	6
Nafion	98	95	50

retained weight of B-SPSN and R-SPSN increased to 103–107% of the original weight, whereas that of Nafion decreased. This is due to the sulfide linkage (−S−) being oxidized to sulfoxide (−SO−) or sulfone (−SO<sub>2</sub>−), which prevented polymer chain degradation due to the hydroxyl radicals.<sup>47,48</sup> However, degradation of polymer chains occurred after 1 h. The B-SPSN maintained 93–95% of their initial weight, while R-SPSN retained 89% after 3 h. In addition, B-SPSN showed a much longer dissolution time (12–15 h) than pristine B-SPSN

(9–11 h), pristine (5 h) (see Table S1), and thermally annealed (6 h) R-SPSN. These results may be due to the lower water uptake of B-SPSN, which could reduce the hydroxyl radical concentration inside the polymer matrix. Consequently, thermal annealing enhanced the chemical stability.

**Electrochemical Performances.** The in-plane and through-plane proton conductivities of B-SPSN and R-SPSN were measured at 80 °C under 30% and 90% RH and compared with those of Nafion, as shown in Figure 6. In

**Figure 6.** In-plane and through-plane proton conductivity of B-SPSN, R-SPSN, and Nafion at 80 °C under (a) 90% and (b) 30% RH.

general, the block copolymers show higher proton conductivity than the random copolymers, especially under low relative humidity conditions due to a well-defined morphology. Though the R-SPSN showed higher proton conductivity than B-SPSN above 90% RH condition due to high water uptake, the proton conductivity of B-SPSN was much higher than that of R-SPSN at 30% RH as expected. In addition, similar to the water diffusion results, the through-plane proton conductivity of B-

SPSN was lower than its in-plane proton conductivity, while R-SPSN showed isotropic proton conduction behavior. Also, the proton conductivity of thermally annealed samples was slightly higher than that of pristine samples. Furthermore, B-SPSN showed a gradual decrease in proton conductivity compared with R-SPSN as relative humidity decreased.

A PEMFC single cell test was performed to evaluate the effects of morphology on fuel cell performance at two different relative humidity conditions (100% and 30% RH). Figure 7

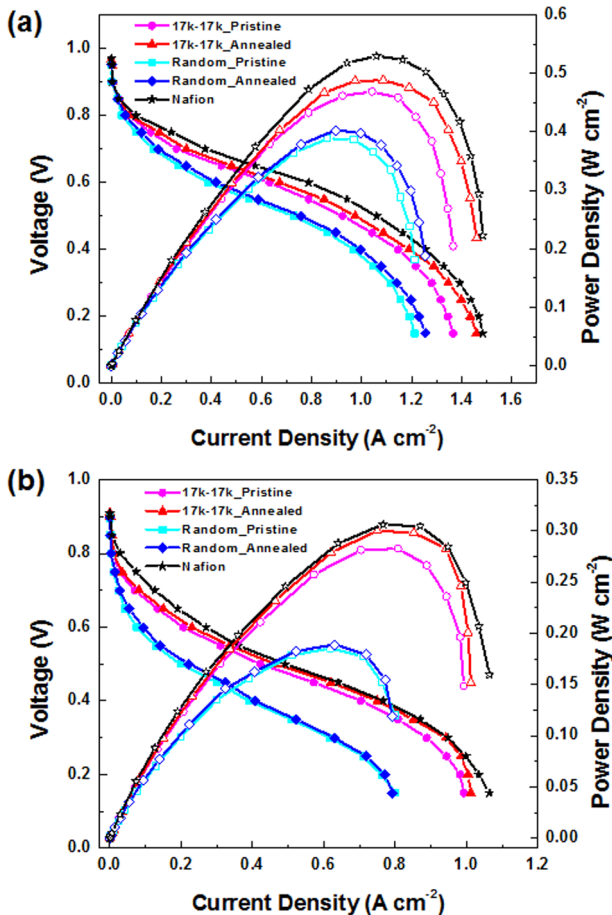


**Figure 7.** PEMFC single cell performances of B-SPSN, R-SPSN, and Nafion at 80 °C under (a) 100% and (b) 30% RH conditions with H<sub>2</sub>/air as a fuel and oxidant.

shows the single cell performance of B-SPSN, R-SPSN, and Nafion. The current density of R-SPSN was 0.418 A cm<sup>-2</sup> at 0.6 V in a fully hydrated state. Although, proton conductivity of R-SPSN was slightly higher than that of B-SPSN, the B-SPSN (0.672 A cm<sup>-2</sup>) showed higher PEMFC performance than R-SPSN due to a well-defined morphology. In addition, the current density of R-SPSN was significantly reduced with a decrease in relative humidity to 30% RH (from 0.418 to 0.094 A cm<sup>-2</sup>), which is a standard test condition of fuel cell vehicle, while B-SPSN (from 0.672 to 0.230 A cm<sup>-2</sup>) and Nafion (from 0.788 to 0.270 A cm<sup>-2</sup>) maintained much of its performance even at low RH conditions. This is due to the ordered morphology of B-SPSN, which leads to effective proton conduction pathways. In spite of the higher proton conductivity of B-SPSN compared to Nafion at 30% RH, B-SPSN exhibited slightly lower single cell performance than Nafion. This is likely due to the capillary phenomena of the small hydrophilic

channel size of Nafion resulting in increased water retention and sorption during fuel cell operation.<sup>43,49</sup> In conclusion, B-SPSN showed promising electrochemical performance as a proton exchange membrane.

## CONCLUSION

We have demonstrated that well-defined lamellar structure formation and nanophase separation were induced in a sulfonated block copolymer containing sulfide linkages and nitrile functional groups due to thermal annealing above  $T_g$  in combination with the shallow rotational energy of the sulfide linkage and the strong dipole–dipole interactions of the nitrile group. Well-ordered hydrophilic ionic channels (lamellar) enhanced proton transport, particularly in the direction parallel to the membrane surface. Thermal annealing decreased water uptake and improved the physical and chemical stability in spite of high IEC values. As a result, thermally annealed B-SPSN showed much higher electrochemical performances than R-SPSN especially at low relative humidity conditions.

## ASSOCIATED CONTENT

### Supporting Information

Physical properties of pristine B-SPSN and R-SPSN. Discussion of minor restricted diffusion effect. This material is available free of charge via the Internet at <http://pubs.acs.org>.

## AUTHOR INFORMATION

### Corresponding Author

\*E-mail: ymlee@hanyang.ac.kr (Y.M.L.).

### Present Addresses

<sup>†</sup>C.H.L.: Department of Energy Engineering, College of Engineering, Dankook University, Cheonan, Korea 330-714.

<sup>#</sup>K.-S.L.: The Sixth Research Team, Daedeok Research Institute, Honam Petrochemical Corp., Daejeon, Korea 305-726.

<sup>%</sup>C.H.P.: ITM-CNR, Universita' della Calabria, Rende, Italy 87030.

### Notes

The authors declare no competing financial interest.

## ACKNOWLEDGMENTS

This work was supported by the New & Renewable Energy R&D program (2008-N-FC12-J-01-2-100), Nano-Material Technology Development program (2012M3A7B4049745) of the National Research Foundation, Ministry of Science and Technology of Korea. This material is based upon work supported by the US National Science Foundation under Awards CHE 1057797 and DMR 0844933. We acknowledge the Advanced Photon Source supported by the U.S. Department of Energy, Office of Science, Office of Basic Energy Sciences, under Contract W-31-109-Eng-38, for access to the beamtime 5ID-D, operated by DND-CAT. The DND-CAT is supported by the E.I. DuPont de Nemours & Co., The Dow Chemical Company, the U.S. National Science Foundation through Grant DMR-9304725, and the State of Illinois through the Department of Commerce and the Board of Higher Education Grant IBHE HECA NWU 96. The diode beam stops were constructed at DuPont by Robert F. Knox and Mark G. Bradigan under J. David Londono's direction.

**■ REFERENCES**

- (1) Li, N.; Wang, C.; Lee, S. Y.; Park, C. H.; Lee, Y. M.; Guiver, M. D. *Angew. Chem., Int. Ed.* **2011**, *50*, 9158.
- (2) Hickner, M. A.; Ghassemi, H.; Kim, Y. S.; Einsla, B. R.; McGrath, J. E. *Chem. Rev.* **2004**, *104*, 4587.
- (3) Zhang, H. W.; Shen, P. K. *Chem. Rev.* **2012**, *112*, 2780.
- (4) Lee, C. H.; McCloskey, B. D.; Cook, J.; Lane, O.; Xie, W.; Freeman, B. D.; Lee, Y. M.; McGrath, J. E. *J. Membr. Sci.* **2012**, *389*, 363.
- (5) Wiles, K. B.; Wang, F.; McGrath, I. E. *J. Polym. Sci., Polym. Chem.* **2005**, *43*, 2964.
- (6) Bae, B.; Miyatake, K.; Watanabe, M. *Macromolecules* **2009**, *42*, 1873.
- (7) Yang, J.; Li, Y. X.; Roy, A.; McGrath, J. E. *Polymer* **2008**, *49*, 5300.
- (8) Asano, N.; Miyatake, K.; Watanabe, M. *Chem. Mater.* **2004**, *16*, 2841.
- (9) Chen, X. B.; Yin, Y.; Chen, P.; Kita, H.; Okamoto, K. I. *J. Membr. Sci.* **2008**, *313*, 106.
- (10) Lee, C. H.; Park, C. H.; Lee, Y. M. *J. Membr. Sci.* **2008**, *313*, 199.
- (11) Li, N. W.; Cui, Z. M.; Zhang, S. B.; Li, S. H.; Zhang, F. *J. Power Sources* **2007**, *172*, 511.
- (12) Park, C. H.; Lee, C. H.; Guiver, M. D.; Lee, Y. M. *Prog. Polym. Sci.* **2011**, *36*, 1443.
- (13) Guo, R. L.; Lane, O.; VanHouten, D.; McGrath, J. E. *Ind. Eng. Chem. Res.* **2010**, *49*, 12125.
- (14) Chen, Y.; Guo, R. L.; Lee, C. H.; Lee, M.; McGrath, J. E. *Int. J. Hydrogen Energy* **2012**, *37*, 6132.
- (15) Badami, A. S.; Roy, A.; Lee, H. S.; Li, Y. X.; McGrath, J. E. *J. Membr. Sci.* **2009**, *328*, 156.
- (16) Hou, J. B.; Li, J.; Madsen, L. A. *Macromolecules* **2010**, *43*, 347.
- (17) Chen, Y.; Lee, C. H.; Rowlett, J. R.; McGrath, J. E. *Polymer* **2012**, *53*, 3143.
- (18) Lee, M.; Park, J. K.; Lee, H. S.; Lane, O.; Moore, R. B.; McGrath, J. E.; Baird, D. G. *Polymer* **2009**, *50*, 6129.
- (19) Einsla, M. L.; Kim, Y. S.; Hawley, M.; Lee, H. S.; McGrath, J. E.; Liu, B. J.; Guiver, M. D.; Pivovar, B. S. *Chem. Mater.* **2008**, *20*, 5636.
- (20) Elabd, Y. A.; Hickner, M. A. *Macromolecules* **2011**, *44*, 1.
- (21) Li, N. W.; Shin, D. W.; Hwang, D. S.; Lee, Y. M.; Guiver, M. D. *Macromolecules* **2010**, *43*, 9810.
- (22) Wang, C. Y.; Li, N.; Shin, D. W.; Lee, S. Y.; Kang, N. R.; Lee, Y. M.; Guiver, M. D. *Macromolecules* **2011**, *44*, 7296.
- (23) Kim, D. S.; Robertson, G. P.; Guiver, M. D. *Macromolecules* **2008**, *41*, 2126.
- (24) Lee, K. S.; Jeong, M. H.; Lee, J. P.; Lee, J. S. *Macromolecules* **2009**, *42*, 584.
- (25) Schuster, M.; de Araujo, C. C.; Atanasov, V.; Andersen, H. T.; Kreuer, K. D.; Maier, J. *Macromolecules* **2009**, *42*, 3129.
- (26) Lee, S. Y.; Kang, N. R.; Shin, D. W.; Lee, C. H.; Lee, K. S.; Guiver, M. D.; Li, N.; Lee, Y. M. *Energy Environ. Sci.* **2012**, *5*, 9795.
- (27) Liu, Y. L. *Polym. Chem.* **2012**, *3*, 1373.
- (28) Borup, R.; Meyers, J.; Pivovar, B.; Kim, Y. S.; Mukundan, R.; Garland, N.; Myers, D.; Wilson, M.; Garzon, F.; Wood, D.; Zelenay, P.; More, K.; Stroh, K.; Zawodzinski, T.; Boncella, J.; McGrath, J. E.; Inaba, M.; Miyatake, K.; Hori, M.; Ota, K.; Ogumi, Z.; Miyata, S.; Nishikata, A.; Siroma, Z.; Uchimoto, Y.; Yasuda, K.; Kimijima, K. I.; Iwashita, N. *Chem. Rev.* **2007**, *107*, 3904.
- (29) Barique, M. A.; Wu, L. B.; Takimoto, N.; Kidena, K.; Ohira, A. J. *Phys. Chem. B* **2009**, *113*, 15921.
- (30) Mullin, S. A.; Teran, A. A.; Yuan, R.; Balsara, N. P. *J. Polym. Sci., Polym. Phys.* **2013**, *51*, 927.
- (31) Lee, C. H.; Lee, K. S.; Lane, O.; McGrath, J. E.; Chen, Y.; Wi, S.; Lee, S. Y.; Lee, Y. M. *RSC Adv.* **2012**, *2*, 1025.
- (32) Takahashi, T.; Hii, S. H.; Sakurai, K. *J. Macromol. Sci., Phys.* **1998**, *B37*, 59.
- (33) Gao, Y.; Robertson, G. P.; Guiver, M. D.; Wang, G.; Jian, X.; Mikhailenko, S. D.; Li, X.; Kaliaguine, S. *J. Membr. Sci.* **2006**, *278*, 26.
- (34) Gao, Y.; Robertson, G. P.; Kim, D. S.; Guiver, M. D.; Mikhailenko, S. D.; Li, X.; Kaliaguine, S. *Macromolecules* **2007**, *40*, 1512.
- (35) Gao, Y.; Robertson, G. P.; Guiver, M. D.; Mikhailenko, S. D.; Li, X.; Kaliaguine, S. *Polymer* **2006**, *47*, 808.
- (36) Shin, D. W.; Lee, S. Y.; Kang, N. R.; Lee, K. H.; Guiver, M. D.; Lee, Y. M. *Macromolecules* **2013**, *46*, 3452.
- (37) Lee, K. S.; Lee, J. S. *Chem. Mater.* **2006**, *18*, 4519.
- (38) Bai, Z. W.; Dang, T. D. *Macromol. Rapid Commun.* **2006**, *27*, 1271.
- (39) Phu, D. S.; Lee, C. H.; Park, C. H.; Lee, S. Y.; Lee, Y. M. *Macromol. Rapid Commun.* **2009**, *30*, 64.
- (40) Li, Y. X.; VanHouten, R. A.; Brink, A. E.; McGrath, J. E. *Polymer* **2008**, *49*, 3014.
- (41) Stejskal, E. O.; Tanner, J. E. *J. Chem. Phys.* **1965**, *42*, 288.
- (42) Kim, Y. S.; Pivovar, B. S. *Annu. Rev. Chem. Biomol.* **2010**, *1*, 123.
- (43) Park, M. J.; Downing, K. H.; Jackson, A.; Gomez, E. D.; Minor, A. M.; Cookson, D.; Weber, A. Z.; Balsara, N. P. *Nano Lett.* **2007**, *7*, 3547.
- (44) Kreuer, K. D.; Paddison, S. J.; Spohr, E.; Schuster, M. *Chem. Rev.* **2004**, *104*, 4637.
- (45) Yan, J. L.; Huang, X. M.; Moore, H. D.; Wang, C. Y.; Hickner, M. A. *Int. J. Hydrogen Energy* **2012**, *37*, 6153.
- (46) Li, J.; Park, J. K.; Moore, R. B.; Madsen, L. A. *Nat. Mater.* **2011**, *10*, 507.
- (47) Zhao, D.; Li, J. H.; Song, M. K.; Yi, B. L.; Zhang, H. M.; Liu, M. L. *Adv. Energy Mater.* **2011**, *1*, 203.
- (48) Weiber, E. A.; Takamuku, S.; Jannasch, P. *Macromolecules* **2013**, *46*, 3476.
- (49) Lee, S. Y.; Shin, D. W.; Wang, C.; Lee, K. H.; Guiver, M. D.; Lee, Y. M. *Electrochem. Commun.* **2013**, *31*, 120.